3D tomographic characterization of sandwich structures

Stefan Dietrich, Kay A. Weidenmann, Peter Elsner

Angaben zur Veröffentlichung / Publication details:

Dietrich, Stefan, Kay A. Weidenmann, and Peter Elsner. 2014. "3D tomographic characterization of sandwich structures." *NDT & E International* 62: 77–84. https://doi.org/10.1016/j.ndteint.2013.12.001.

3D tomographic characterization of sandwich structures

Stefan Dietrich [a,*], Kay Weidenmann [a], Peter Elsner [b]

[a] Institute of Applied Materials, Karlsruhe Institute of Technology, Germany
[b] Fraunhofer Institute for Chemical Technology, Germany

1. Introduction

The application of computed tomography (CT) in the field of NDT has proven to be especially useful in the investigation of micro- and meso-structures of composite materials [1]. Furthermore the realization of a three-dimensional representation of the structural composition allows, in contrast to traditional radiographic methods, the exact location of failure zones and irregularities. Due to the mostly lightweight composite structures and therefore the easy penetrability of X-rays several drawbacks of conventional tomography in material science like artefacts or sample thickness restrictions can be neglected. Since the fundamental mathematics for a simple reconstruction of the absorption contrast of an object from its 2D projections have been established in the 1980s [2,3], the implementation into modern computer hardware today additionally allows for high resolution and wide field of view imaging. Modern μ-CT-systems with a focal spot size in the few micrometer range in combination with high dynamic range flat panel detectors provide a resolution down to 1 µm [4].

The application of a μ-CT-analysis in the field of composite characterization is widespread. In case of fiber reinforced polymer matrix composites the spatial distribution and identification of single filaments, fiber bundles or fabric composition has been achieved (see e.g. [5]). For single fibers and fiber networks the fiber orientation and packing can be used to numerically model or calculate both conductive and mechanical properties of the composite [6,7]. For braided composites it is possible to characterize the shape and deformation in order to provide a realistic and micro-structurally exact input into finite element simulations [8].

For foam or resin components in composite matrices or adhesive joints especially the pore content is regularly analysed by μ-CT measurements and is implemented as a standard operation in most μ-CT analysis software packages. Furthermore it is also feasible to detect the pore shape and position to account for stress and strain effects beyond simple volumetric descriptions in the modelling of mechanical properties [9]. Recently even the in situ characterization of composites has been possible [10,11] providing the ability of 3D strain field measurements from μ-CT data.

Nonetheless for sandwich components or hybrid lightweight structures there have been only few studies investigating the entire structure and not only single components. The focus in these studies has been mainly the qualitative assessment of structural properties as well as the investigation of failure initiation and failure progress [12]. The advantages of μ-CT in the investigation of the core-face-sheet interface with respect to porosity could be first outlined in [13]. There the important advantages of the μ-CT measurement methods have been

* Corresponding author.
E-mail address: stefan.dietrich@kit.edu (S. Dietrich).

highlighted and applied to different problems concerning sandwich material selection and design. One of these problems is the field of the non-destructive testing of impact events. The detection and shape description of deformations and delaminations in the vicinity of the impact point is essential for the investigation of damage evolution and damage mechanisms and has been employed by X-ray and microscopic 2D techniques in the last decades (see e.g. [14]). Here computed tomography provides a versatile tool-set for the characterization of the impact zone and the damage to the internal microstructure and mesostructure on a representative 3D basis [15,16].

However the analysis of the image data for hybrid material structures or lightweight composites often lacks the automation and comparability for a quantitative depiction of micro- and mesostructures or damage classification. At the same time the role of processing and handling is often not incorporated into the evaluation of the sandwich components which may otherwise reveal a close coupling between geometry, shape and microstructure formation. In this work we outline three methods with exemplary applications to honeycomb GFRP-sandwiches from an integral spray moulding technique. The goal of these methods is the automatic evaluation of user-defined characteristics and their representation in a form that explicitly reveals the relations between process setup and structural properties which determine the mechanical quality in the field of application.

2. Material and methods

2.1. Material properties, processing and mechanical testing

Sandwich composites are a combination of a stiff face-sheet carrying the tensile and compression load in the skin layer and a supporting core component separating the outer layers and bearing shear deformations. This combination offers an optimized bending stiffness of the entire structure. The sandwich manufacturing process is based on the recently developed, fully automated spray manufacturing of sandwich shell elements for automobile and railway vehicles. Therein the infiltration of the fiber architecture in the chopped strand mat (CSM) is simultaneous with the adhesion to the core component due to the penetration of excess polyurethane (PU) foam from the matrix into the open core cavities (see Fig. 1). A detailed description of the process parameters, polyurethane system and comprehensive mechanical properties of the sandwich can be found in [17–19]. The sandwich configurations investigated herein consist of a sinusoidal or hexagonal paperboard core with a 0.35 mm thick face-sheet layer.

The investigated face-sheet is build up from a CSM with a fiber volume fraction of 31% and an average strand length of 50 mm. The investigated core components are sinusoidal paperboard honeycombs (testliner paper 115 g/m^2) with a volume density of 57 kg/m^3 and hexagonal Nomex honeycombs ECA-I 4.8-32 [20]. The sinusoidal cell geometry, as provided by the manufacturer, is 8.97×4.97 mm^2 with a wall thickness of 180 μm. The core height in the initial state is 20 mm. For the polyurethane (PU) matrix deposition on the face-sheet an amount of 1160 g/m^2 was sufficient to achieve a rigid connection between face-sheet and core. The processing steps for the composite sandwich include the sandwich preforming of the face-sheet on the core and a subsequent robot controlled spraying with a low viscosity polyurethane system. The positioning in the compression mold and curing of the PU matrix at an elevated mould temperature of 150 °C finalize the process chain (see Fig. 2).

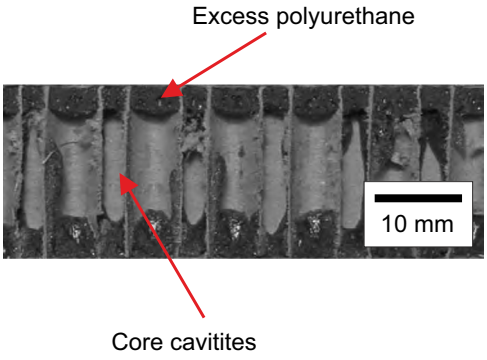

Fig. 1. Micrograph of the infiltrated core cavities for sinusoidal honeycomb cores.

For the impact testing of the sinusoidal sandwich an Instron Dynatup drop tower with a drop cage weight of 5.24 kg has been used. The impact energy was calibrated to 5, 10 and 20 J. The quadratic (140×140 mm^2) sandwich samples were clamped between two metallic plates with a circular cut-out of 100 mm diameter. The samples were struck at the center by a hemispherical indenter fixed on a load cell underneath the drop cage.

2.2. Computed tomography

The measurement process for tomographic data can be divided into two main tasks. Usually in a laboratory source radiographic projections are taken for a fixed angle increment over 360°. In a subsequent step the projections are reconstructed using the FDK algorithm [2] to obtain three dimensional image data sets. The μ-CT measurements of different sandwich samples have been conducted on an YXLON Y.CT Precision μ-CT System. The X-ray tube was operated at an acceleration voltage between 90 and 145 keV with a target current of 0.03–0.06 mA on a tungsten transmission target. The scanner gantry was set up in such a way as to obtain a maximum resolution (20–70 μm) whilst preserving the representative sample volume according to the characterization tasks. The reconstructed data sets from 2010 projections have a volume edge length of 2048 pixels and a varying volumetric picture element (voxel) size according to Table 1.

The projection data and the reconstructed slices of the 3D volume are finally stored as 16-bit 2D image stacks providing raw data with a size of approximately 32 Gb for the visualization and image analysis on a workstation equipped with four Xeon Quad-Core CPUs and 96 Gb of RAM as well as sufficient graphics hardware.

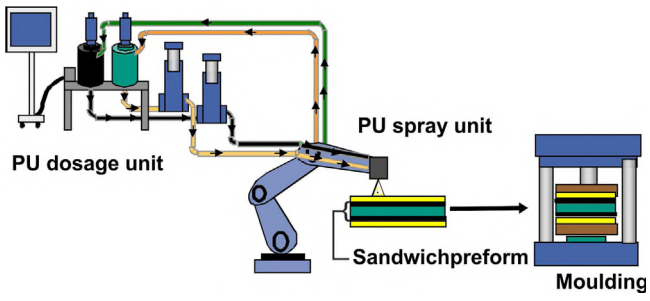

Fig. 2. Illustration of the integral processing steps.

Table 1
Setup of the μ-CT-system for the different measurement tasks.

Application	Voxel size (μm)	Voltage (kV)	Current (mA)
Core cell geometry/Wall thickness	20.3	95.0	0.05
Roving orientation	31.0	90.0	0.03
Impact damage	69.0	148.0	0.06

3. Calculation

The analysis of the 3D data was carried out with visualization and measurement routines comprising a combination of commercial and open-source software tools. The structural analysis of periodicity and build-up for the honeycomb cells in the core component has been carried out using a combination of VSG Avizo Fire® and Matlab®. The image processing steps include the identification of the gluing zones of the sinusoidal wall to the straight liner wall by thickness discrimination in the segmented image (see Fig. 3). For the hexagonal core geometry the extraction of the triple points in the lattice using morphological skeletonization provides a unique characteristic of the cell extent in combination with the measurement of the neighbourhood distance distribution. The centroidal axis of the gluing column shows no significant directional deviation and therefore the cell deformation is estimated from the mean distance between neighbouring centroidal axes (see Fig. 3).

The thickness analysis of the liner in the entire 3D core structure was accomplished using the ImageJ [21] plugin developed in [22] which is predicated by the publications of e.g. Hildebrand [23]. Therein the local thickness is defined and calculated based on the minimal encompassed sphere of an arbitrary 3D object. The local thickness information was statistically concentrated on a distribution of relative frequency where the minimum voxel size acts as the lower boundary and resolution limit. The fiber orientation estimation algorithm is based on the works of Wirjadi et al. [24,25] and has been implemented for the scope of this paper using the C++ 3D imaging library ITK [26]. Therein an anisotropic Gauss filtering process is applied to the segmented image data and the filter response for different relative roving and filter orientations is used as a reference for the local roving orientation in each voxel (see Fig. 4).

The appropriate Gauss filter size has been derived from the mean roving diameter and has an aspect ratio of 1:3 with a short half-axis of approximately 10 µm. For the segmentation of all images the global thresholding method after Otsu [27] is used. The code is made publicly available under the open source project Composight [28] by the authors.

4. Results

The results extracted by the image analysis procedure can be used separately to provide information on the process factors influencing the component microstructure. Additionally we incorporate the information on the raw material state of the sandwich components into the image analysis of samples altered through small mass impact events to demonstrate the usefulness of the extracted information beyond microstructure characterization. Following the characterization of the core and face-sheet configuration during the process we emphasize on the damage detection aspects of impact loading.

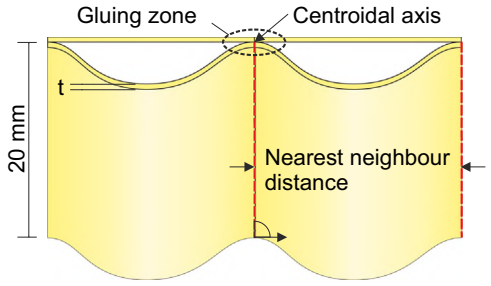

Fig. 3. Schematic of the image analysis algorithms for honeycomb cell geometry.

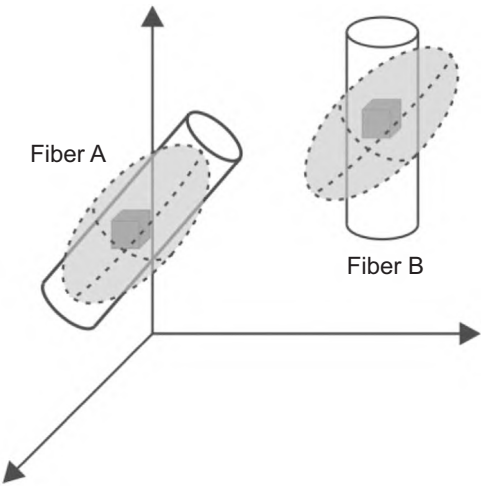

Fig. 4. Fiber orientation estimation using anisotropic Gauss filters.

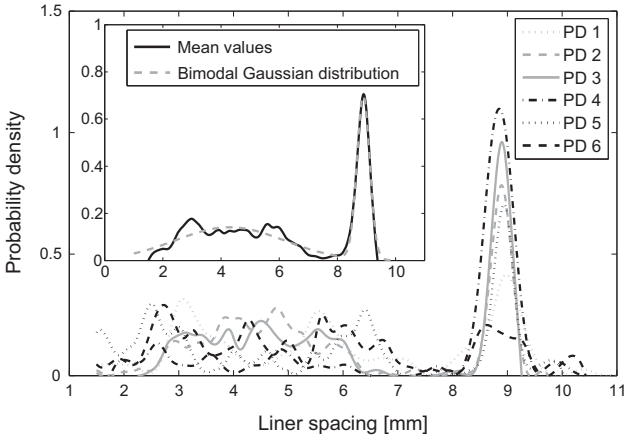

Fig. 5. Distribution functions for all 6 samples and their overall mean.

4.1. Core geometry

The definition of cell regularity and cell extent could be justified via μ-CT measurements on 6 samples with a size of $60 \times 60\ mm^2$ in comparison with measurements based on the manufacturer data. The cell shapes as well as the adhesive paths expose a strong deviation resulting in non-optimal arrangement of the cell walls under pressure loading. This effect can be accounted for by the extraction of a statistically descriptive distribution function of the distance between neighbouring adhesive layers as plotted in Fig. 5.

Herein the relative cell displacement can be as much as half of the cell size while the deviation of the cell shape from the sine wave form in the orthogonal direction is only marginally visible. It is evident from Fig. 6 that a broad variation of non-optimal cell stacking exists in the core samples. The original μ-CT-data of a low resolution axial slice of the core then translates into the according labelled (coloured) gluing zones identified through a thickness threshold.

Furthermore there is a pronounced peak representing the targeted cell size of the manufacturer at 8.97 mm. The cell wall thickness and irregularities are fundamental properties for the pressure load capacity and damage evolution in the core component. This is especially important in the case of adhesive bonding of paper bulk material without subsequent dipping into polymeric resin because the columns along the double walled adhesive paths

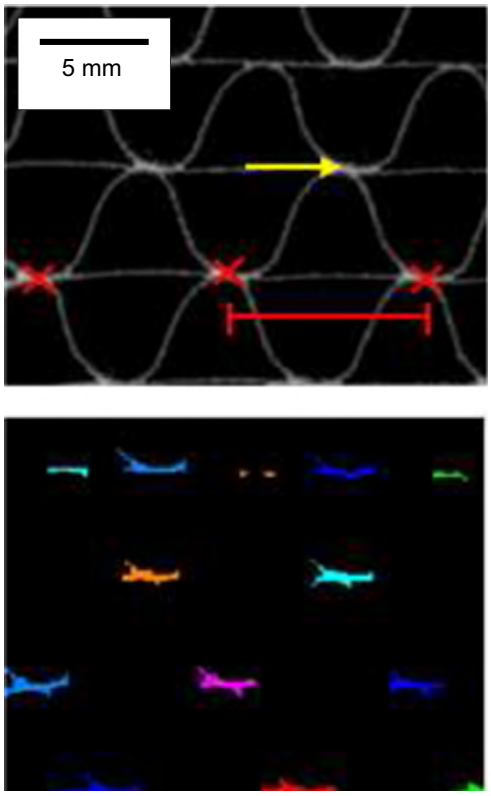

Fig. 6. Detection of gluing zones defining the geometry and extent of the individual cells in the periodic arrangement of sinusoidal honeycomb cores.

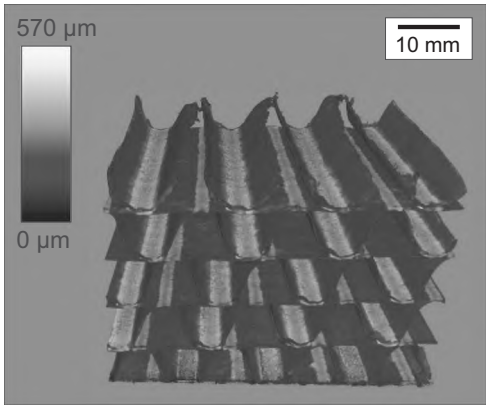

Fig. 7. Visualization of the liner thickness enabling the detection of the gluing paths and the measurement of local thickness.

can contribute substantially to the overall stiffness and strength of the core structure.

With the aforementioned methods the local thickness in a region of interest (ROI) of the sinusoidal core was detected (see Fig. 7). The 4 samples for this measurement had a length of 160 mm and a width of 4 complete sinusoidal cells with a core height of 20 mm. The extracted cumulative distribution function of the detected cell wall thicknesses in one sample is represented in Fig. 8.

By this thickness measurement the relative amount of wall thicknesses present in a sandwich core can be assessed and implemented into strength calculations which are of particular importance in the design process and characterization of cell geometries and cell wall materials [29]. For the hexagonal cell array a similar approach for the detection of the cell regularity is applied to quantify the wall length distributions. Because of the

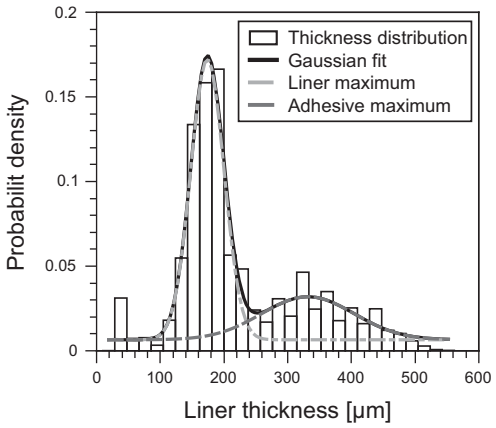

Fig. 8. Probability distribution of the liner thickness for a core sample of 50 cells including Gaussian distributions for the liner wall and the double walled gluing zone.

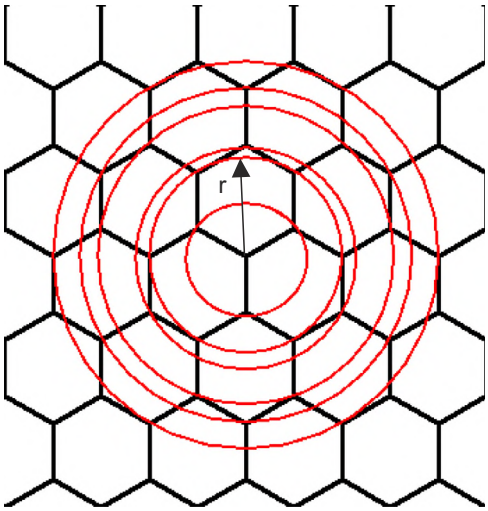

Fig. 9. Edge length detection through triple points in a hexagonal core lattice.

hexagonal symmetry all directions in the lattice can be sampled and measured by detecting the lattice triple-points (see Fig. 9).

The measurements of the hexagonal cell deviations via triple points were carried out slice by slice, for each cell triple point as center of the detection algorithm, along the core thickness direction. A sample mean value over all slices was calculated for the detected lengths per cell corner as indicated in the histogram of Fig. 10. The radial distribution of the next neighbours in the lattice indicates variations around the optimal distances based on the manufacturer cell size (see Fig. 10). The broadening of the distance peaks represents deformations of the cells and the splitting of peaks around the optimal position indicates an anisotropic deformation introduced during processing or handling.

One important information deduced form the μ-CT-analysis of the core structure as produced by the manufacturer is the sufficient regularity along the core height. Therefore the assumption of insignificant skew of the cell structure at different core heights can be justified. This is a fundamental fact necessary for the evaluation of core damage based on the lateral displacement of the cell walls in the damage zone compared to the undisturbed core regions.

4.2. Face-sheet micro-structure

The microstructure and roving architecture in the CSM indicates a distinct modification during the moulding process. The

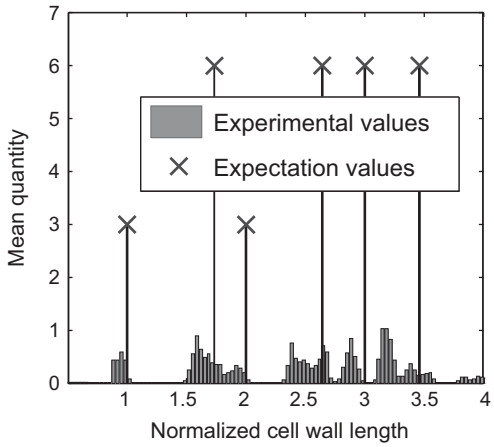

Fig. 10. Corresponding radial distance distribution for the nearest neighbours in a normalized representation.

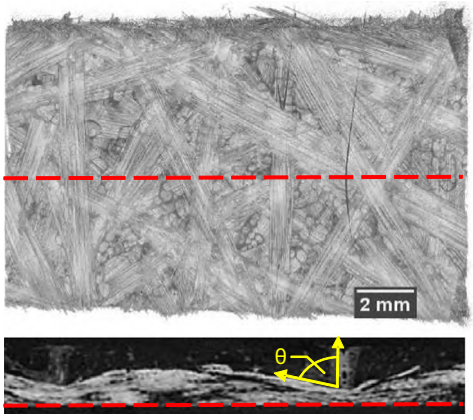

Fig. 11. Top view as well as median plane of the spray infiltrated face-sheet.

fiber orientation near the core interface is altered due to the indentation of the cell walls into the resilient CSM against the mould tool wall (see Fig. 11).

The comparison of the infiltrated and the raw CSM additionally illustrates the foaming of the PU matrix between the strands which is primarily responsible for the load partition and strength in the face-sheet (compare Figs. 11 and 12).

The analysis of the out-of-plane orientation component for the strands in the infiltrated face-sheet can best be visualized by a spherical orientation distribution function (ODF) as indicated in Fig. 13.

Therein the relative volume fraction pointing in different directions can be read from the intensity value on the sphere surface (see Fig. 14). The comparison of the distribution function with the expected equatorial plane $\theta=90^\circ$ can be used to determine the transversely symmetric alignment of strands. A single parameter indicating the mean out-of-plane angle θ and a constant distribution in the plane ($\phi=$const.) proves to be adequate for a quantitative description by an analytic distribution function (see e.g. [30]).

As a result, the mean value of the full width at half maximum is at $\theta=65^\circ$, with no strand orientations measured below 34° (see Fig. 14). The orientation analysis has been carried out for different face-sheet areal weights and shows a strong interaction with the mould pressure and raw CSM thickness. The influence of the face-sheet thickness indicates a decreasing overall out-of-plane orientation for thicker CSM. Therefore the rising pressure at the core wall face-sheet joint for thicker CSM translates into a kinking of

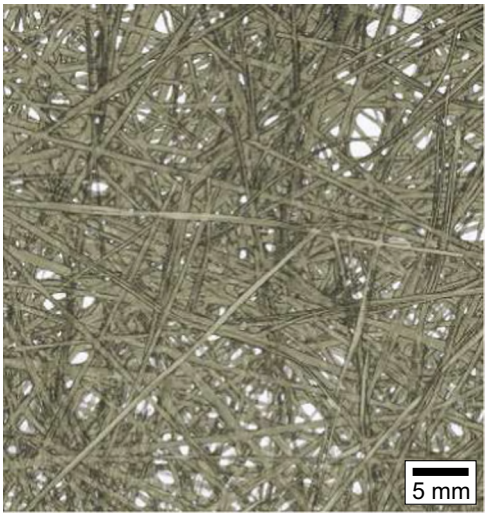

Fig. 12. Detailed axial view on the raw chopped strand mat.

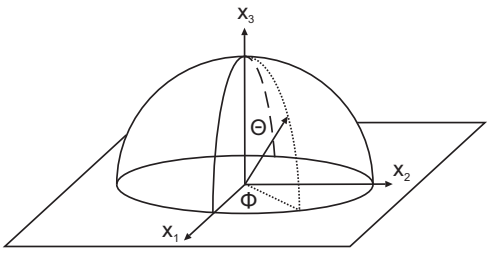

Fig. 13. Definition of the out-of-plane angle θ and in-plane angle ϕ in the face-sheet plane.

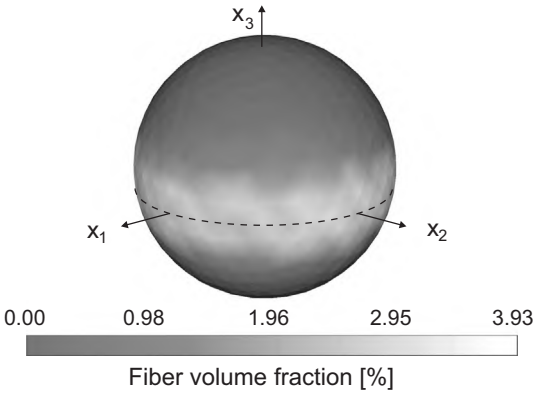

Fig. 14. Orientation distribution histogram with the relative volume fraction in percent visualized as intensity values.

the cell wall edges and shows a reduced subsequent raising of the strands from their planar orientation (see Fig. 11).

4.3. Impact testing

The evaluation of damage during impact events shows a unique advantage of a μ-CT measurement in the easy and unaltered measurement principle compared to the conventional destructive or tactical damage assessment. The combination of results from previous sections provides fundamental knowledge for a precise characterization of impact damage extent due to low velocity impact events. Therefore the altered roving orientation and cell geometry variation pose a lower limit of deviations present in the intact sandwich structure. Stronger deviations of these

characteristics indicate the damage zones introduced under varying impact loading.

For the three tested impact energies the typical load-deflection curves of the sinusoidal core sandwich are plotted in Fig. 15. The comparison of the peak loads for both core materials shows an increasing variance for higher impact energies with a plateau behavior of the simultaneously rising peak loads (see Fig. 16).

From the image median slices at different impact energies the onset of damage in the sandwich composite can be assessed (see Fig. 17). It is obvious that through the PU foam connection between face-sheet and core the initiation of damage in the core cell walls is distributed and passed into the inner, PU-free region. Therefore the damage zone extends substantially further into the core as expected from the apparent surface indentation and causes a reduced stiffness and strength of the entire structure already at small impact energies. A striking characteristic of the damage zone is the core deformation by buckling and kinking of the cell walls which is transmitted by the PU grouting well before an indentation of the face-sheet becomes visible (see Fig. 17).

To account for the introduced damage influencing the overall stability of the sandwich the boundary of the deformed region was found by digital image correlation of the 3D volume with an undisturbed slice of the core material. Therefore the minimum correlation intensity in Fig. 18 corresponds to deformed cell walls. The damage boundary can be represented by a surface fit as in Fig. 19 where the detected defect points are chosen at a correlation grey value threshold of $T=208$ (8-bit scaling, see Fig. 18). For a closed form descriptor the surface can be enveloped by an ellipsoidal hull (see Fig. 20).

The extracted geometric values from image analysis are given in Fig. 21 for the three samples presented in Fig. 17 as a function of the impact energy.

The caliper ratios of the damage zone extent in x- and y-direction (see Fig. 20) show a rather constant trend of the radial size of the zone $R_X = f_x/c_x$. This indicates that the initial core damage introduced in the early impact stages is independent of impact velocity and energy.

The linear increase in the through thickness ratio $R_Y = f_y/c_y$ assigned to the indentation of the face-sheet is directly related to the rise in peak load for increasing energies. The first drop in the linearly increasing load-deflection history during the impact event

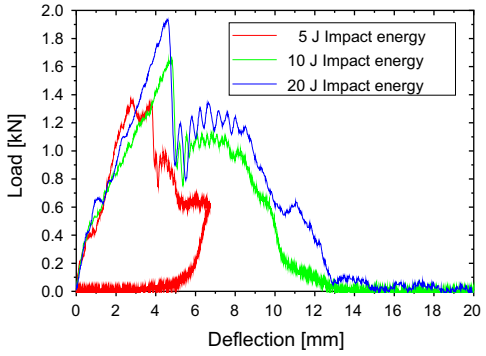

Fig. 15. Comparison of load-deflection curves for three impact energies.

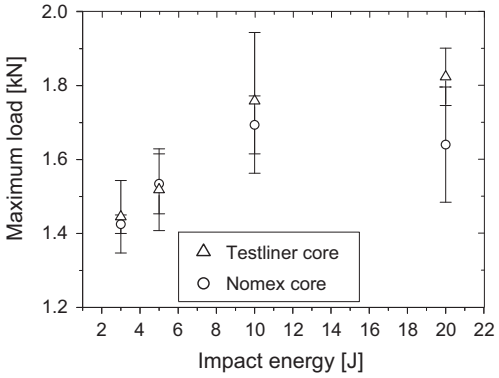

Fig. 16. Peak load value for sandwiches produced from both core types at all tested energies.

Fig. 18. Assessment of the damage introduced underneath the deformed face-sheet in the core structure. Visualization is for one transversal slice as an iso-line plot of image correlation grey-values with a slice of intact core cells in the same sample. T indicates the selected grey value threshold for the damage zone surface.

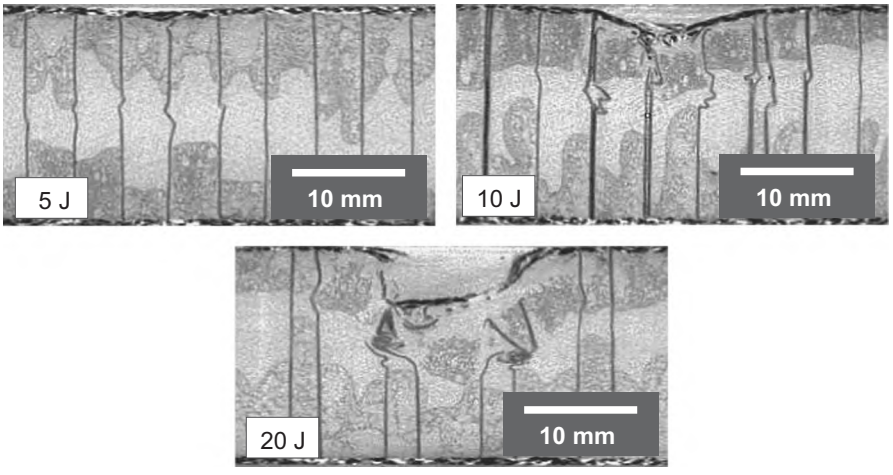

Fig. 17. Median plane of three impacted sandwich samples for different impact energies (5–20 J) indicating the onset of damage in the face-sheet and in the surrounding core material.

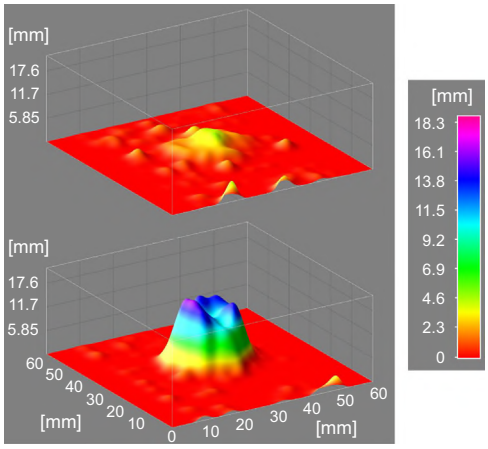

Fig. 19. Surfaces of the indented face-sheet and the core damage zone.

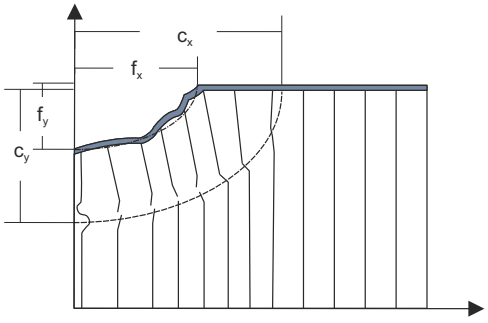

Fig. 20. Schematic of the definition of the damage zones in the face-sheet and the core.

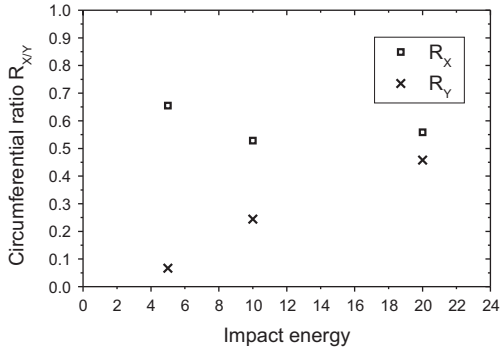

Fig. 21. R_X/R_Y ratios of the elliptical circumference derived from a least-square fit of the damage zone borders detected in the images.

appears for all impact energies at approximately 0.8–1.0 mm (see Fig. 15) and may therefore be directly correlated with the constant core wall buckling length and constant core damage area c_x (see Figs. 17 and 21).

5. Discussion

The control of manufacturer supplied honeycomb cores for geometric variations and inhomogeneities was carried out using core type specific, geometric characteristics whose variations and distribution could be statistically extracted from tomographic 3D image data. These measures show broad variations in cell geometry and shape in the lateral direction but indicate a uniform cell position along the core height. Additionally the possibility of a measurement of thickness scatter in the cell walls expressed through a Gaussian distribution can be expected to contribute immensely to the core crush strength prediction as already indicated by other authors from 2D measurements [29]. Preliminary simple calculations based on a plate buckling approach for the cell walls show a rising of approximately 15% in the compression strength using our realistic geometric distribution functions. The methods for the quality assessment of core components presented herein can also be included into a post-processing program where a random sampling and extensive inspection is necessary (e.g. aerospace quality assurance). Here the covered μ-CT measurements and image analysis procedures provide a fast and rigorous data acquisition and handling especially suitable for inaccessible structural details.

The measurement of variations of strand orientation in the face-sheet during this study was carried out on a centimetre scale representing several cells for a global modelling approach. The view at intra-cell changes however reveals a strong core geometry dependence not resolved with our measurements. Therefore further investigations need to be conducted for the correlation and coupling of single core cell geometry with roving elevation (see Fig. 22) which would introduce significant local orthotropy of the face-sheet.

Additionally the three dimensional fiber orientation analysis simultaneously reveals the flaws in measurement and interpretation of standard mechanical sandwich testing like e.g. flexure beam tests on integrally produced sandwich structures. The properties of the processing chain prohibit the development of a homogeneous thickness and promote a foamed and graded geometry of the face-sheet to core transition. Especially for the material manufactured with the herein mentioned method the mechanical tests can be revised in order to gain correct material properties. Due to the high resolution measurements and the resulting time of data handling and analysis the investigation of roving properties in the face-sheet qualifies for a comprehensive process control and material design investigation. The automatically extracted single parameter orientation distribution function (ODF) can be used in subsequent modelling steps providing information on real microstructure as the basis of an analytic or finite element model of mechanical properties (see e.g. [7]). This structural information is also essential to identify process-microstructure relations for a correlation of process parameters with elastic and plastic mechanical properties.

The evaluation of damage in low velocity impact events using an automated measurement routine for the geometry and shape parameters of the damage zone in the μ-CT images was possible for the entire range of impact energies. The reduction of the analysed surface and bounding area to scalar parameters by fitting of a geometric primitive (ellipsoid) allows to compare damage characteristics for impact energies. The μ-CT images emphasize several mechanisms of the impact damage inherent to the integral production method. The limits of the damage initiation value strongly depend on the position of the first indenter contact and the consequent deformation of the first cell walls which is strongly correlated with the state of the PU-rich sub-layer. The strength of the core partition within the outer core damage area mapped on the crushing strength of the core material from static compression tests leads to a maximum load of ≈ 750 N. For the inner damage region directly underneath the dented face-sheet the projected

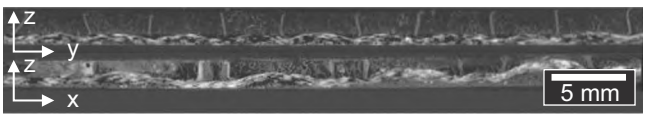

Fig. 22. Formation of the face-sheet through the imprinted cell walls in different directions of the sinusoidal core.

maximum load is ≈250 N. Both values represent the upper and the lower bound for the experimentally measured load drop as pointed out in Fig. 15. While the lower value coincides well with static indentation results of the same sample and indenter geometry indicating a mean value of the load drop around 200 N it is obvious that for a concise picture of the damage sequence the geometry of the PU sub-layer and the dependencies of the indenter impact point location need to be included into the investigation. Therefore the μ-CT analysis provides a very versatile tool for extensive impact testing programs. These cover the material sample stage as well as entire sandwich parts considering the restrictions of geometry and resolution limit for the μ-CT system and the materials internal structures.

6. Conclusions

In this study several methods for a quantitative analysis and description of μ-CT results collected to characterize the meso- and micro-structure of sandwich composites are outlined. In contrast to traditional 2D techniques the coupling between structural features can be easily accessed by 3D imaging techniques. Nonetheless the comparison of the tomographic images with high resolution 2D images is imperative to avoid frequent errors of the image processing and analysis steps. The investigated problems comprise the cell and wall material variation of honeycomb sandwich cores, the process dependent formation of irregularities in the GFRP face-sheet as well as the quantitative assessment of the failure zone induced during impact. The evaluation through distribution functions allows for a thorough description of the different characteristics which can be used both to control and regulate the production process of sandwich components and sandwich structures. Furthermore it is possible to use these results as basis for an exact analytical or numerical analysis of mechanical features like elastic/plastic deformation, buckling and impact delamination phenomena. Based on the realistic structural properties and the extraction of damage zones the tomographic imaging techniques provide the possibility to support both experiments and modelling with a comprehensive 3D understanding. The special focus towards an automated analysis procedure in combination with the non-destructive sample preparation attains the goal of an objective and statistically firm investigation of the material properties at hand. These aspects clearly show the versatility of μ-CT investigations in process control and design as well as high-throughput material and damage characterization.

Acknowledgments

These investigations were carried out through the research activities of the KITe hyLITE Plus project. This project is funded by the European Union through the program European Funds for Regional Development as well as state government of Baden-Württemberg in Germany.

References

[1] Baruchel J, Buffière J, Maire E, Merle P, Peix G. X-ray tomography in material science. Paris, France: Hermes Science; 2000.
[2] Feldkamp I, Davis IC, Kress JW. Practical cone-beam algorithm. J Opt Soc Am A 1984;1:612–9.
[3] Kak AC, Slaney M. Principles of computerized tomographic imaging. New York, USA: IEEE Press; 1988.
[4] Mayo S, Miller P, Wilkins S, Gao D, Gureyev T. Laboratory-based X-ray microtomography with submicron resolution. In: Optics & photonics, international society for optics and photonics, 2006, p. 63181E.
[5] Eberhardt CN, Clarke AR. Automated reconstruction of curvilinear fibres from 3d datasets acquired by x-ray microtomography. J Microsc 2002;206 (1):41–53.
[6] Faessel M, Delise C, Bos F, Castra P. 3d modelling of random cellulosic fibrous networks based on x-ray tomography and image analysis. Compos Sci Technol 2005;65(13):1931–40.
[7] Dietrich S, Gebert J, Stasiuk G, Wanner A, Weidenmann K, Deutschmann O, et al. Microstructure characterization of CVI-densified carbon/carbon composites with various fiber distributions. Compos Sci Technol 2012;72(15):1892–900.
[8] Badel P, Vidal-Salle E, Maire E, Boisse P. Simulation and tomography analysis of textile composite reinforcement deformation at the mesoscopic scale. Compos Sci Technol 2008;68(12):2433–40.
[9] Drach B, Tsukrov I, Gross T, Dietrich S, Weidenmann K, Piat R, et al. Numerical modeling of carbon/carbon composites with nanotextured matrix and 3d pores of irregular shapes. Int J Solids Struct 2011;48(18):2447–57.
[10] Elliott J, Windle A, Hobdell J, Eeckhaut G, Oldman R, Ludwig W, et al. In-situ deformation of an open-cell flexible polyurethane foam characterised by 3d computed microtomography. J Mater Sci 2002;37(8):1547–55.
[11] Adrien J, Maire E, Gimenez N, Sauvant-Moynot V. Experimental study of the compression behaviour of syntactic foams by in situ X-ray tomography. Acta Mater 2007;55(5):1667–79.
[12] Salvo L, Belestin P, Maire E, Jacquesson M, Vecchionacci C, Boller E, et al. Structure and mechanical properties of AFS sandwiches studied by in-situ compression tests in X-ray microtomography. Adv Eng Mater 2004;6 (6):411–5.
[13] Davies P, Choqueuse D, Bourbouze G. Micro-tomography to study high-performance sandwich structures. J Sandw Struct Mater 2011;13(1):7–21.
[14] Bernard ML, Lagace PA. Impact resistance of composite sandwich plates. J Reinforced Plast Compos 1989;8(5):432–45.
[15] Crupi V, Epasto G, Guglielmino E. Low-velocity impact strength of sandwich materials. J Sandw Struct Mater 2011;13(4):409–26.
[16] Crupi V, Epasto G, Guglielmino E. Computed tomography analysis of damage in composites subjected to impact loading. Frattura Integr Strutt 2011;17:32–41.
[17] Kuppinger J, Weidenmann K, Kordick M, Wafzig F, Henning F, Elsner P. Influence of fibre length and concentration on the mechanical properties of long glass fibre reinforced polyurethane. J Plast Technol 2010;5:205–27.
[18] Kuppinger J, Weidenmann K, Haspel B, Wafzig F, Henning F, Elsner P. Influence of processing conditions, fiber contents and fiber lengths on fiber orientation in the polyurethane fiber spraying process. J Plast Technol 2011;6:44–65.
[19] Kuppinger J. Material- und Prozessvalidierung zur Herstellung faserverstärkter Polyurethanbauteile im Fasersprühverfahren [Ph.D. thesis]. Karlsruher Institut für Technologie; 2012.
[20] Kronauer B. ECA-I Honeycomb—technical datasheet. Technical Report EC 536-68e/06-08, EURO-COMPOSITES; June 2008.
[21] Abramoff M, Magelhaes P, Ram S. Image processing with imagej. Biophotonics Int 2004;11(7):36–42.
[22] Dougherty R, Kunzelmann K. Computing local thickness of 3d structures with imagej. Microsc Microanal 2007;13(S02):1678–9.
[23] Hildebrand T, Rüegsegger P. A new method for the model-independent assessment of thickness in three-dimensional images. J Microsc 1997;185 (1):67–75.
[24] Robb K, Wirjadi O, Schladitz K. Fiber orientation estimation from 3d image data: practical algorithms, visualization, and interpretation. In: Proceedings of the 7th international conference on hybrid intelligent systems. Washington, DC, USA: IEEE Computer Society;2007, p. 320–5.
[25] Wirjadi O. Models and algorithms for image-based analysis of microstructures [Ph.D. thesis]. Fachbereich Informatik der Technischen Universität Kaiserslautern; 2009.
[26] Ibanez L, Schroeder W, Ng L, Cates J, et al. The ITK software guide. 2nd ed. New York, USA: Kitware Inc; 2005.
[27] Otsu N. A threshold selection method from gray-level histograms. Automatica 1975;11(285–296):23–7.
[28] Dietrich S, Bertram B. Composight open source project, Online, 12, 2011. URL ⟨http://sourceforge.net/apps/mediawiki/composight/⟩.
[29] Pohl A. Strengthened corrugated paper honeycomb for application in structural elements [Ph.D. thesis]. ETH Zurich; 2009.
[30] Schjødt-Thomsen J, Pyrz R. The mori–tanaka stiffness tensor: diagonal symmetry, complex fibre orientations and non-dilute volume fractions. Mech Mater 2001;33(10):531–44.